Separation and Purification Technology 378 (2025) 134567

Contents lists available at ScienceDirect

Separation and Purification Technology

journal homepage: www.elsevier.com/locate/seppur

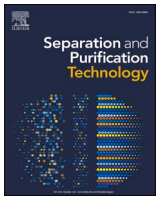

Development of cation-exchange membranes using solvent-free 3D printing: Towards tailored surface topographies

Mekhna Venu [a], Claudia F. Galinha [a], João G. Crespo [a,b], Sylwin Pawlowski [a,*]

[a] LAQV-REQUIMTE, DQ, FCT, Universidade NOVA de Lisboa, 2829-516 Caparica, Portugal
[b] Instituto de Tecnologia Química e Biológica António Xavier, Universidade NOVA de Lisboa, Av. da República, 2780-157 Oeiras, Portugal

ARTICLE INFO

Editor: Dr. B. Van der Bruggen

Keywords:
Ion exchange membranes
Profiled membranes
Additive manufacturing
Electrical resistance
Permselectivity
Sulfonation

ABSTRACT

Electromembrane processes are employed in critical applications such as desalination, lithium recovery, and salinity gradient energy conversion. However, issues like fouling and concentration polarisation may limit their effectiveness. Profiled ion-exchange membranes offer several advantages over flat membranes, including improved fluid mixing, enhanced mass transfer, lower pressure drop (thus, lower energy consumption), and elimination of the spacer's shadow effect. Nonetheless, their preparation is considerably more complex than that of flat membranes. In this study, we pioneered the use of solvent-free fused deposition modelling (FDM) 3D printing to fabricate flat and profiled (chevron and stripe) cation-exchange membranes (CEMs). The functionalisation of the 3D-printed membranes into CEMs was achieved via sulfonation. The optimised electrical resistance and permselectivity of the prepared membranes were 10.7 ± 4 Ωcm^2 and 97.3 ± 4 %, respectively, after 14 h of sulfonation, closely matching commercial alternatives (e.g., FUMASEP FKB-PK-130, 9.7 ± 3 Ωcm^2 and 96.7 ± 1 %). Sulfonation durations exceeding 14 h increased the membranes' electrical resistance due to the formation of sulfone cross-bridges that do not participate in cations' exchange. Since FDM 3D printing is a solvent-free and additive manufacturing method, it significantly reduces waste during membrane fabrication, resulting in an E-factor value of 1.5. Therefore, this work opens a path toward customisable, scalable, and greener CEM production for electrochemical applications ranging from the recovery of critical raw materials and water desalination to renewable energy conversion.

1. Introduction

According to the EU decarbonisation strategy, electrification of industry is one of the critical aspects, since the easiest way to use carbon-free renewable energy is to convert it into electricity [1]. Electromembrane processes such as electrodialysis (ED) [2,3], membrane capacitive deionisation (MCDI) [4,5], flow electrode capacitive deionisation (FCDI) [6–9], and electrolysis (EL) [10] are direct electricity users without the need for its conversion into other driving forces, such as pressure or temperature gradients. They have been applied in diverse areas, such as water desalination, lithium recovery and CO_2 use. On the other hand, reverse electrodialysis (RED) can harvest salinity gradient energy released from a mixture of two streams with different salinities [11–13]. However, while membrane processes in general are widely considered green and sustainable due to the reduced energy input, the production of membranes might not be environmentally friendly, resulting in the generation of between 100 and 500 L of wastewater contaminated with toxic solvents for each square metre of membrane produced [14,15].

The most common arrangement of electromembrane stacks is a plate-and-frame configuration, in which spacers separate flat ion exchange membranes (IEMs) to create internal channels. Several studies have shown that replacing flat IEMs with profiled IEMs can have advantages such as higher mass transfer and lower pressure drop, reducing the limitations caused by concentration polarisation, fouling and spacers shadow effect [16]. For instance, the use of profiled cation-exchange membranes in diffusion dialysis (DD) for amino acid separation showed an 8-fold increase in phenylalanine flux compared to flat membranes [17]. This was attributed to the increased surface area and improved hydrodynamics, which reduced the diffusion layer thickness and facilitated more efficient mass transfer [17]. In reverse electrodialysis, the use of chevron-profiled IEMs [18] led to 8–14 % higher net power density compared to stacks with flat IEMs [19] and a 30 % reduction in ohmic resistance when using ridge-profiled membranes

* Corresponding author.
E-mail address: s.pawlowski@fct.unl.pt (S. Pawlowski).

https://doi.org/10.1016/j.seppur.2025.134567
Received 13 June 2025; Received in revised form 24 July 2025; Accepted 30 July 2025
Available online 31 July 2025

[20]. However, the preparation and design of such profiled IEMs are limited by fabrication methods, namely thermal pressing [19,20], since only thermally stable polymers can be used, and the respective equipment costs are high [21–23]. Furthermore, a new mould has to be fabricated each time a new design is to be explored, making it time-consuming. Therefore, there arises a need for more adaptable, green and efficient fabrication of profiled IEMs.

3D printing offers the ability to fabricate structures with intricate and highly customisable geometries, including precise surface profiles [24,25]. Regarding the preparation of ion exchange membranes (IEMs), there are very few studies focused on this subject. Table SI.3 in the Supporting Information compares IEMs produced by digital light processing (DLP), stereolithography (SLA), and fused deposition modelling (FDM) (this work) 3D printing techniques. The use of DLP 3D printing, combined with quaternisation, allowed the preparation of flat anion exchange membranes (AEMs) with a Cl^-/SO_4^{2-} selectivity of 24.0 [26]. In another study, SLA 3D printing was used to prepare flat heterogeneous cation exchange membranes by combining photo-curable and cation exchange resins, resulting in membranes with an ion exchange capacity of 2.23 meq/g and a resistivity of 2200 Ωcm [27]. By using custom photolithography, similar to SLA, micropatterned anion-exchange membranes (AEMs) were prepared with an ion exchange capacity of up to 1.63 meq/g [28] and resistivity of around 960 Ωcm [29]. However, dimension and shape discrepancies were noticed due to errors in the SLA printing process, such as light bleeding and overcuring, emphasising the importance of optimising the 3D printing process for membrane fabrication. In FDM 3D printing, a thermoplastic polymer filament is melted and deposited layer by layer onto a printer bed in the desired shape. Unlike the earlier explored SLA or DLP 3D printing techniques, which require specialised photocurable resins that are harmful to the environment and also reduce the chemical and mechanical durability of the fabricated membranes, FDM uses no solvent or resin. Nonetheless, despite all these advantages, no studies have been performed on manufacturing ion exchange membranes using this method.

Thus, in this work, solvent-free FDM 3D printing was employed for the first time to fabricate flat and profiled cation-exchange membranes (CEMs). First, the process was optimised while printing flat membranes, and afterwards, chevron- and stripe-profiled membranes were also prepared. The influence of sulfonation time on membrane chemical structure was elucidated by X-ray photoelectron spectroscopy, demonstrating and explaining why there is an optimal sulfonation time. The permselectivity and electrical resistance of the fabricated 3D-printed CEMs were compared against a commercial CEM.

2. Materials and methods

2.1. Preparation of membranes

Membranes were prepared following a two-step procedure: 3D printing and functionalisation for obtaining cation exchange membranes through sulfonation. First, flat membranes were 3D printed to optimise printing and sulfonation procedures, after which profiled membranes, with chevron and stripe corrugations, were fabricated by the optimised method. The flat membranes were circular with 40 mm diameter and 0.24 mm thickness. The base of profiled membranes was also circular with a 40 mm diameter and 0.20 mm thickness, with chevron profiles on top with a width of 0.02 mm, height of 0.25 mm and distance between them of 3 mm, or with stripe profiles with a width of 0.02 mm, height 0.25 mm and distance between them of 4 mm. The respective designs can be seen in Figure SI.1 in the Supporting Information.

2.1.1. 3D printing

After an assessment of different available commercial filaments, aiming their sulfonation while keeping good chemical and mechanical stability, the Flexfill TPE 90A filament (Filamentum, Czech Republic), a combination of a polyolefin and styrene-ethylene-butylene (SEBS), was chosen to print the membranes. The thermoplastic elastomer (TPE) polymer has high tear resistance, layer adhesion and flexibility. The interpolymer nature of TPE provides two polymer domains, which makes it mechanically and chemically strong. The aromatic rings of SEBS hold positions for functional group attachment (as shown in Figure SI.2a in the Supporting Information) [30,31]. The membranes were printed using a MK4S 3D Printer (Prusa, Czech Republic). The nozzle and bed temperatures were 240 °C and 60 °C, respectively.

2.1.2. Functionalisation (sulfonation)

The 3D-printed membranes were immersed in a sulfonating agent of 1:3 chlorosulfonic acid (97 % purity, Sigma-Aldrich): 1,2- dichloroethane (99.9 % purity, Sigma-Aldrich) solution at a temperature of 25 ± 0.2 °C. Sulfonation of the flat membranes was carried out for different periods: 2, 6, 10, 14, 18 and 24 h. The resulting membranes were named as STPE2, STPE6, STPE10, STPE14, STPE18, STPE24, respectively. The pristine membrane (0 h of sulfonation) was named USTPE. The chevron and stripe profiled membranes were sulfonated for 14 h (this optimal time was determined when preparing flat membranes). The sulfonated membranes were then neutralised in 20 % w/w aqueous solution of NaOH (99.9 % purity, Sigma-Aldrich) for 24 h.

2.2. Characterisation of membranes

2.2.1. Mechanical strength analysis

The mechanical properties of membranes were analysed by determining the elongation percentage, the yield point, and the fracture point using a texture analyser equipment (TAXT plus, Stable Micro Systems, England) with 5 kg as the cell load. Membrane strips of 60 mm × 20 mm were clamped between the grips of the texture analyser with a crosshead speed of 1 mm/s for the analysis.

2.2.2. Water content

The water content (w%) of membranes was calculated by their immersion in deionised water at room temperature for 24 h. Membranes were weighed on a microbalance after removing any excess of water from the surface. The dry membranes were prepared by vacuum drying overnight at 40 °C. The percentage of water content (w%) was determined as:

$$w\% = \frac{w_w - w_d}{w_d} \times 100 \quad (1)$$

where w_d(g) and w_w(g) are the mass of the dry and the after-immersion membranes, respectively.

2.2.3. Water contact angle

The hydrophilicity of membranes was examined by measuring the static contact angle using a Drop Shape Analyser DSA25 (KRÜSS, Germany). A droplet of distilled water (3 μL) was gently dispensed, using a syringe, on the membrane surface (dried previously with filter paper). The reported contact angle is the average of measurements with three water droplets at different locations, at room temperature.

2.2.4. Thermogravimetric analysis (TGA) and differential scanning calorimetry (DSC) analysis

To analyse the thermal properties of membranes, a thermal analyser STA 449 F3 Jupiter (Netzsch, Germany) was employed using a ramp of 10 °C/min in the temperature range of 0–550 °C under a nitrogen atmosphere with a flow rate of 40 mL/min. Samples of approximately 5 mg weight were placed in the aluminium pan for analysis.

2.2.5. Fourier transform infrared spectroscopy (FT-IR)

Fourier Transform Infrared Spectra (FT-IR) with attenuated total reflectance (ATR) mode was used to determine the surface chemistry of membranes. The equipment was a Bruker Spectrometer IFS 66/S FT-IR instrument (USA) equipped with H-ATR and ZnSe crystal. Membranes were dried with filter paper before obtaining the measurements. Analysis was performed at various positions of membranes over both sides to assess homogeneity in chemical bonding. If no significant difference was noticed, a single analysis was considered. The normalised spectra were recorded in the range of wave numbers from 400 to 4000 cm^{-1} at a resolution of 4 cm^{-1} with 14 scans per sample.

2.2.6. Ion exchange capacity

For the ion exchange capacity (IEC) measurement, membranes were equilibrated in a 1 mol/L NaCl (99.9 % purity, Sigma-Aldrich) aqueous solution for 48 h to ensure a complete ion exchange between Na^+ ions in the salt solution and H^+ ions associated with the membrane sulfonic groups. Due to ion exchange, the acidic membrane is converted to its sodium form, and the pH of the solution decreases. The amount of released H^+ was determined by titration against a 0.02 mol/L NaOH (99.9 % purity, Sigma-Aldrich) solution. An average value from 5 measurements was taken as the result:

$$IEC(\mathrm{meq/g}) = \frac{V_{NaOH} \times M_{NaOH}}{W_{dry}} \times 100\%$$

where N_{NaOH} (meq/l), V_{NaOH} (l), and W_{dry} (g) are the concentration, the consumed volume of NaOH solution and the weight of the dried film, respectively.

2.2.7. Degree of sulfonation

The degree of sulfonation (DS) of membranes was calculated using the following equation [32]:

$$DS(\%) = \frac{M_p \times IEC}{1000 - (M_f \times IEC)}$$

where IEC (meq/g) is the ion exchange capacity, M_p is the molecular weight of the unsulfonated polymer repeating unit (which was assumed as 194000 g/mol [33]) and M_f is the molecular weight of the sulfonic acid group (81 g/mol).

2.2.8. Electrical resistance

The electrical resistance of membranes was measured in a home-made 3D-printed six-compartment cell. The details about its construction and set-up can be found in Section 3 of the Supporting Information. The current–voltage curves were obtained through linear sweep voltammetry measurements with a 10 mV/s scan rate and a potential step of 10 mV in the range of ± 0.05 V. Vertex 5A potentiostat (Ivium Technologies, The Netherlands) was used as the power source. First, the measurements were performed in a cell with the membrane under study to obtain the combined resistance of solution and membrane (R_{m+s}) (Ω) as described by equation 4:

$$R_{m+s} = \frac{U}{i}$$

where U is the voltage drop measured between the electrodes (V) and i is the current (A). To obtain the membrane resistance, the resistance due to the solution must be subtracted from the combined resistance. The solution resistance was calculated by performing the steps mentioned above but in a cell without the central membrane under study [34].

2.2.9. Permselectivity

The permselectivity (α) of each membrane was calculated as the ratio between measured (v_m) and theoretical potential difference (v_t) as described by equation 5:

$$\alpha = \frac{v_m}{v_t} \times 100$$

The experimental potential difference was measured in open circuit voltage (OCV) mode in a two-compartment cell (the details about its construction and set-up can be found in Section 4 of the Supporting Information) using a Vertex 5A potentiostat (Ivium Technologies, The Netherlands).

The theoretical potential difference was calculated from the Nernst equation (eq. 6), assuming membrane permselectivity (α) as 100 % [34]:

$$v_t = \frac{\alpha RT}{zF} \ln\left(\frac{a_{con}}{a_{dil}}\right)$$

where R is the universal gas constant (8.314 J mol^{-1} K^{-1}), T is the temperature in Kelvin (K), z is the valency of the ion, F is the Faraday's constant (96485 C mol^{-1}), a_{con} and a_{dil} are the activities of the concentrated and diluted solution, respectively.

2.2.10. X-ray photoelectron spectroscopy (XPS)

The XPS analysis of membrane surfaces and cross-sections was performed with a Kratos Axis Supra (Kratos Analytical, UK), using monochromated Al Kα irradiation (1486.6 eV). Scans were acquired with an X-ray power of 150 W, and pass energies of 180 eV (wide scans) and 10 eV (detail scans). The membranes were mounted in an aluminium crucible and showed charge accumulation during the measurement. Charge neutralisation with an electron flood gun was employed, and the lowest binding energy component of C 1 s was referenced at 284.8 eV in CasaXPS, which was the software used for data analysis.

2.2.11. Scanning electron microscopy with energy dispersive spectroscopy (SEM-EDS)

The morphology of the profiled membranes was analysed via scanning electron microscopy (SEM) Hitachi TM4000Plus II (Japan), with an accelerating voltage of 5 kV, SE (secondary electron) as the image signal and 85x magnification. The presence and distribution of sulfur, sodium, and chlorine in flat membranes were confirmed by energy-dispersive spectroscopy using an X-ray detector (Oxford, model INCA 150) by Hitachi Regulus 8220 Scanning Electron Microscope (Mito, Japan). Membranes were coated with an Au/Pd film of 15 nm thickness using a Sputter Quorum.

3. Results and discussion

3.1. Membrane preparation and their mechanical properties

Fig. 1 shows (a) USTPE (unsulfonated membrane), (b) STPE2 (2 h of sulfonation), (c) STPE14 (14 h of sulfonation) and (d) STPE24 (24 h of sulfonation) flat membranes fabricated in this study by FDM 3D printing. The discussion about profiled membranes is done in section 3.3.

The physical dimensions of the produced membranes are summarised in Table SI.1 in the Supporting Information. The average thickness of the 3D-printed flat membranes (0.25 mm) was very similar to the targeted thickness (0.24 mm, as designed in the.stl file), indicating that the FDM 3D printing technique accurately produced objects with the required membrane geometry. After sulfonation, the average thickness increased by 0.01 mm (~4%) due to swelling.

To quantitatively assess their mechanical properties, elongation percentage, fracture strength and yield point were determined. The elongation percentage for flat membranes was in the range of 104 % – 435 % with a fracture strength above 3.6 MPa, indicating they have high elasticity and high fracture strength. The yield points of USTPE, STPE2, STPE14 and STPE24 membranes were 2.29 MPa, 2.17 MPa, 2.08 MPa and 1.87 MPa (with error value of ± 50 Pa) respectively, confirming their exceptional mechanical strength. In practical terms, the membrane samples used in mechanical tests could be stretched between 4 and 17

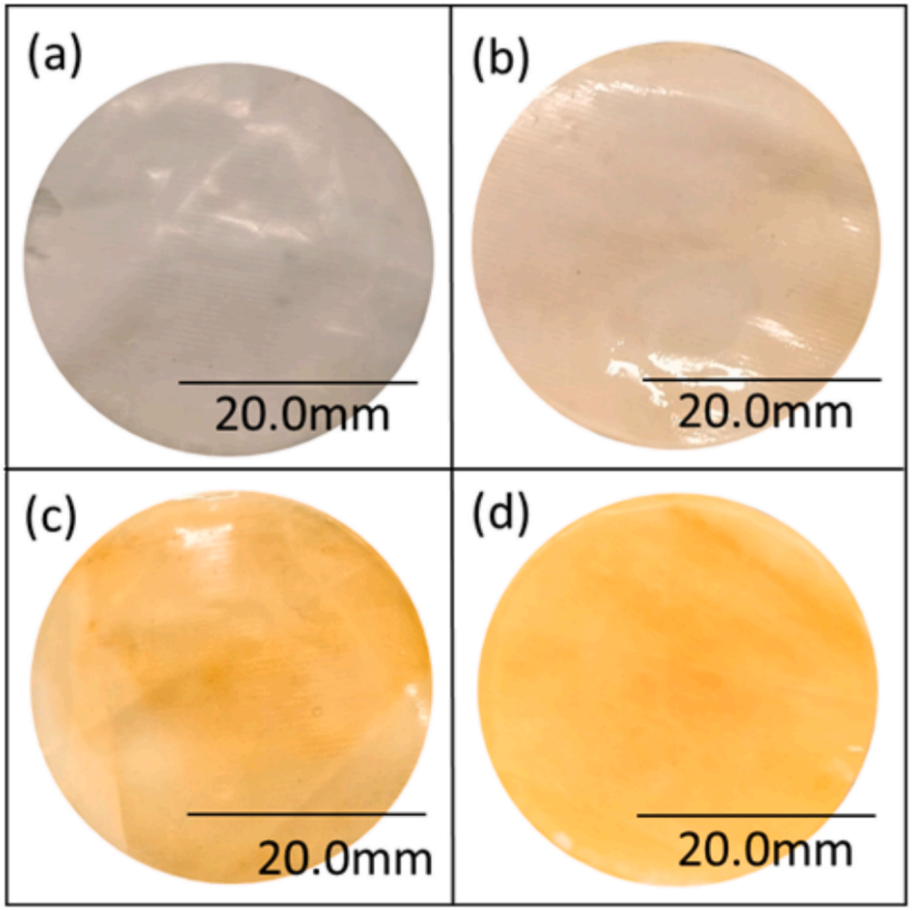

Fig. 1. Photos of (a) USTPE, (b) STPE2, (c) STPE14 and (d) STPE24 3D-printed flat membranes.

cm before breaking, which is clearly above any possible deformation that might occur in any electromembrane process application.

3.2. Characterisation of flat membranes

3.2.1. Water content and contact angle

The water content (Fig. 2 (a)) and contact angle (Fig. 2 (b)) of the fabricated flat membranes increased from 10 to 90 % and decreased from 74° to 26°, respectively, with the increase in sulfonation time.

The water contact angle measurement showcases that the hydrophobicity of the interpolymer backbone decreased with the incorporation of hydrophilic sulfonic acid functional groups. However, since only the hydrophilic domain (SO_3H) of the nano-structure is capable of becoming hydrated in the presence of water, there is a probability of dissociation of some sulfonic acid groups from the polymer backbone into the aqueous solution as the polymer becomes hydrated. This might lead to the degradation of characteristics such as stability and mechanical properties, according to the literature [35–37]. Nevertheless, the mechanical tests performed on these membranes (section 3.1) show that even the membranes with 24 h of sulfonation have good mechanical properties. On the other hand, appropriate membrane hydrophilicity and water content must be maintained to ensure high cations conductivity within the ionic network of the sulfonated polymer membranes.

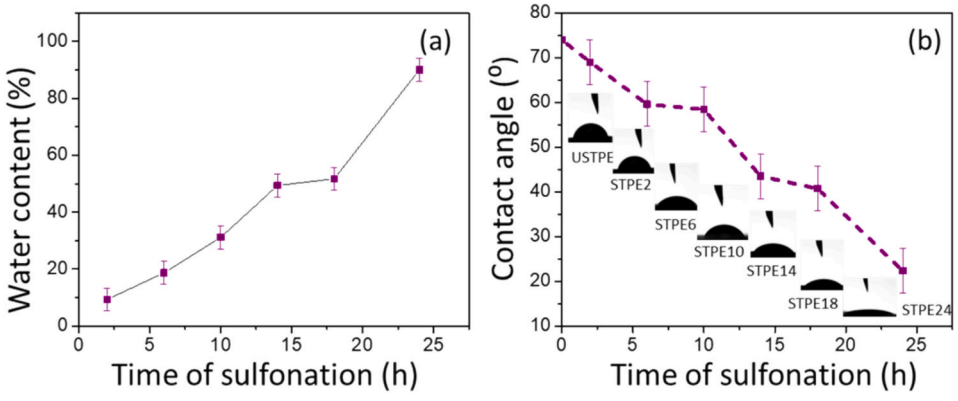

Fig. 2. (a) Water content and (b) water contact angle of the prepared flat membranes.

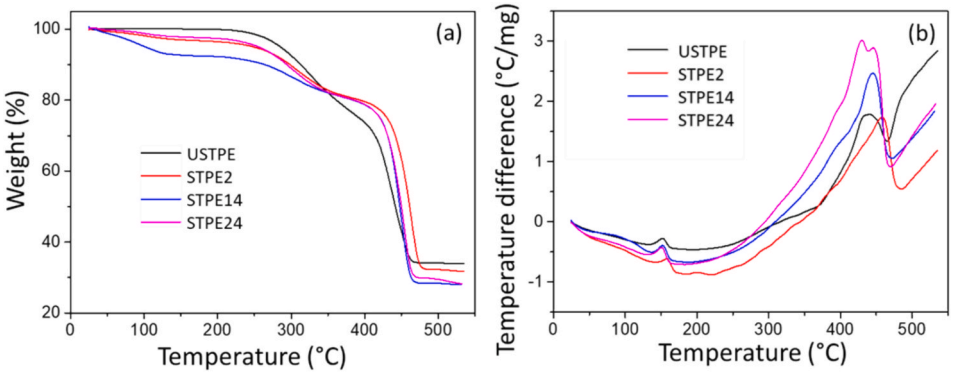

Fig. 3. (a) Thermogravimetric analysis (TGA) and (b) Differential scanning calorimetry (DSC) of USTPE, STPE2, STPE14 and STPE 24 membranes.

3.2.2. *Thermogravimetric analysis (TGA) and differential scanning calorimetry (DSC)*

The thermal degradation behaviour of flat membranes was investigated by TGA. The weight loss of the membranes as a function of temperature is shown in Fig. 3a. From the three major peaks observed, it can be concluded that membranes undergo three distinct weight-loss stages. The first degradation started around 100 °C due to the evaporation of water molecules trapped in the interpolymer mesh and those attached to the sulfonic acid group. STPE14 membrane has more water weight loss (8.3 %) than STPE2 and STPE24 membranes (3.2 % and 2.6 %, respectively). This might be due to the difference in how water molecules are trapped inside the membranes. The results suggest that water molecules in STEP14 are more easily removed, while for STPE24 the water is more deeply involved in solvation interactions with other chemical groups within the material and, therefore, more structured and less free. The second weight loss in the range of 150–250 °C was attributed to the desulfonation of the STPEs membranes, as this weight loss is absent in the case of the USTPE membrane. The highest degree of degradation for the STPE14 membrane in this range might indicate the presence of more sulfonic acid groups, which will be explained in detail in section 3.2.5. The third stage of weight loss between 250–380 °C is associated with the thermal degradation of the aromatic rings of the -styrene blocks. Above 400 °C occurs the final degradation of the interpolymer backbone. The obtained results agree with earlier studies that found that all sulfonated styrene-ethylene-butylene membranes exhibited three major degradation steps [35,38]. The thermal behaviour of membranes was also characterised by DSC (Fig. 3b). The membranes had two endothermic peaks. The first broad peak between 130 and 160 °C corresponds to the material's glass transition temperature (T_g), which is in the previously reported range for styrene block in TPE polymer [39]. Moreover, as the temperature increased, the above-mentioned interpolymer demonstrated broadening in peak area compared to the USTPE membrane from 150 to 180 °C. As previously explained, this peak may be ascribed to the evaporation of residual water in the hydration shell of the sulfonate groups, hence it lacks for the USTPE membrane. The distinct, split into two domains peak of the STPE24 membrane might indicate a difference in sulfone structure bound to the interpolymer (R_2SO_2 and RSO_3Na), which is discussed in detail in section 3.2.5. Simultaneously, it is also observed that the peak height increases with an increase in sulfonation time, indicating an increased amount of sulfone in the membranes.

3.2.3. *Fourier Transform Infrared spectroscopy (FTIR) characterisation*

According to previous studies [35,36,38,40], FTIR characteristic peaks of the TPE polymer are at 2850–2920 cm^{-1}, while peaks near 1350–1342 cm^{-1} and 1165–1150 cm^{-1} are due to the presence of the sulfonic acid group in the membranes. Moreover, the intense and broadened band in the region of 1250–1150 cm^{-1} is due to the asymmetric stretching vibration of S=O (forms of sulfone), and the sharp

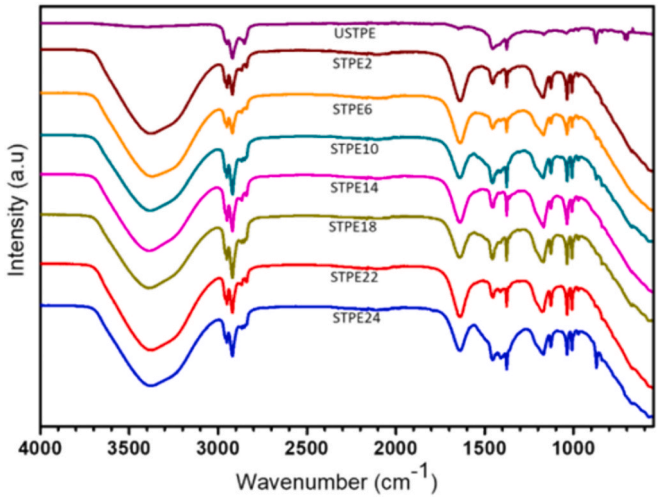

Fig. 4. FTIR spectra of prepared flat membranes.

absorption peaks at 1100–1000 cm^{-1} are due to the symmetric stretching vibration of S=O. All of them can be observed at FTIR spectra of the prepared sulfonated membranes (Fig. 4). Therefore, it indicates that the sulfonic acid groups were grafted onto the *para*-position of the SEBS block of the TPE polymer.

3.2.4. *Electrochemical properties*

Fig. 5 shows the main electrochemical properties of prepared flat membranes: degree of sulfonation, ion exchange capacity, electrical resistance and permselectivity.

The ion exchange capacity (IEC) represents the amount of fixed ionic charges per unit mass of the membrane. The sulfonic acid groups in the membrane were determined by potentiometric titration owing to the acid-base neutralisation reaction [41]. The IEC increased with an increase in sulfonation time to 14 h (Fig. 5a). For the STPE14 membrane, it reached the highest value of 2.8 meq/g; thereafter, with a further increase in sulfonation time, the IEC started to decrease. The unexpected value out of trend for the STPE10 membrane might result from a relatively high error value of ± 0.7 meq/g. A similar trend was observed for the degree of sulfonation (Fig. 5a), which reached a maximum value of 70 % (error value of ± 10 %) for the STPE14 membrane. These results show that, despite the increase in sulfonation time, the membrane sulfonated during 14 h reached the highest degree of sulfonation and IEC, which will be discussed in detail in section 3.2.5.

The degree of sulfonation and ion exchange capacity strongly influence the permselectivity and resistance of the membrane. The results show that the electrical resistance decreases to 10.7 ± 4 Ωcm^2, and permselectivity increases to 97.3 ± 4 % till the 14 h of sulfonation

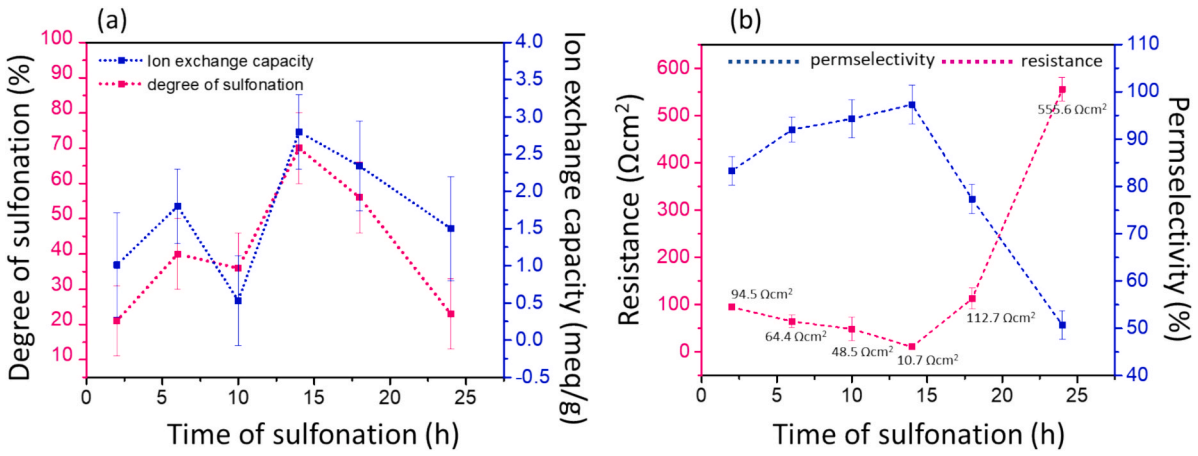

Fig. 5. (a) Degree of sulfonation and ion exchange capacity and (b) electrical resistance and permselectivity of prepared membranes vs time of their sulfonation. (For comparison, the commercial cation exchange membrane (FUMASEP® FKB-PK-130) has an electrical resistance of 9.7 ± 3 Ωcm^2 and permselectivity of 96.7 ± 1 %). Average values and error bars were calculated based on at least 3 replicates of the membranes.

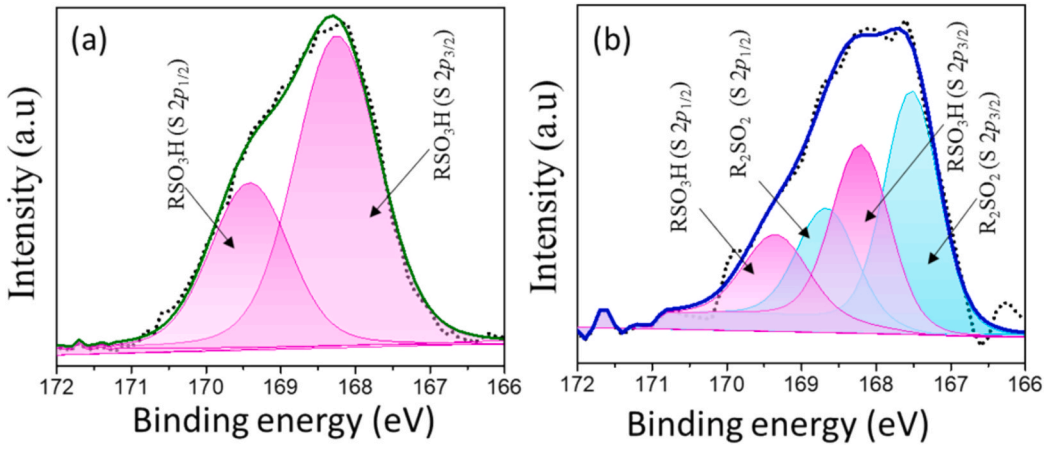

Fig. 6. Sulfur 2p XPS spectrum of (a) STPE14 and (b) STPE24 membranes. The dotted line corresponds to experimental data points, while the green and blue lines correspond to fitted curves resulting from simulated peaks.

(Fig. 5b). These values are comparable to the commercial cation exchange membrane (FUMASEP® FKB-PK-130) with an electrical resistance value of 9.7 ± 3 Ωcm^2 and permselectivity of 96.7 ± 1 % and are much better than those of recycled ion-exchange membranes (56 Ωcm^2 and 65 %, respectively) [42]. It is also important to note that the 3D-printed sulfonated membranes were 0.26 mm thick, whereas the thickness of the commercial membrane was 0.15 mm, which is almost half. Hence, the resistivity of the sulfonated 3D-printed membrane is lower than that of the commercial membranes (412 vs. 647 Ωcm). This material property offers an exciting starting point for future optimisation of 3D-printed membranes, especially if the reduction of their thickness becomes possible (which depends on 3D printers' capabilities). As the resistance of the prepared STPE14 and the commercial membrane is very similar, the cation flux was also practically the same for both (Figure SI.5 in the Supporting Information). For membranes with more than 14 h of sulfonation, an increase in the resistance and a decrease in the permselectivity is observed with the increase of sulfonation time. One of the major reasons for this phenomenon can be sulfone cross-bridging (Figure SI.2b in Supporting Information), which may occur due to high exposure time towards chlorosulfonic acid during sulfonation [43]. This phenomenon is further discussed with the help of XPS spectra, in the next section (Section 3.2.5).

3.2.5. *Trend of resistance and permselectivity explained through XPS*

Fig. 6a shows the S 2*p* XPS spectra of the STPE14 membrane, which portrays a single kind of sulfone bond present within the membrane, which represents S 2$p_{3/2}$ and S 2$p_{1/2}$ peaks of RSO_3H with an oxidation state + 6, in the region of 169.31 eV. In Fig. 6b, the sulfur 2p XPS spectra of the STPE24 membrane show four peaks, which correspond to S 2$p_{3/2}$ and S 2$p_{1/2}$ of RSO_3H and S 2$p_{3/2}$ and S 2$p_{1/2}$ of R_2SO_2. Even though the S 2$p_{3/2}$ peak falls under the + 6 oxidation state, one of them shifts from 168.17 to a lower binding energy value of 167.5 eV, which indicates the presence of both the sulfonic acid group and the sulfone cross-bridge. In the structure of the sulfone cross-bridge (Figure SI.2b in the Supporting Information), since one of the oxygens is replaced with carbon, which has lesser electronegativity, the XPS peak S 2*p* shifts to a lower binding energy. The results clearly indicate the presence of a single chemical state for sulfur in the STPE14 membrane, which is the sulfonic acid group, and two chemical states of sulfur for the STPE24 membrane, which are the sulfonic acid group and the sulfone cross-bridge.

The sulfonic acid group, in the presence of strong electrophiles like chlorosulfonic acid, can be alkylated at the O or the S atom. Pearson's hard/soft acid/base (HSAB) concept provides insight into the direction of alkylation. Among the O and S, the S, which is the soft nucleophilic centre, is more easily deformed by electrophiles than the O electron shell. This S-alkylation leads to sulfone formation between two aryl rings [39,44,45]. The addition of a sulfonating medium is a highly exothermic

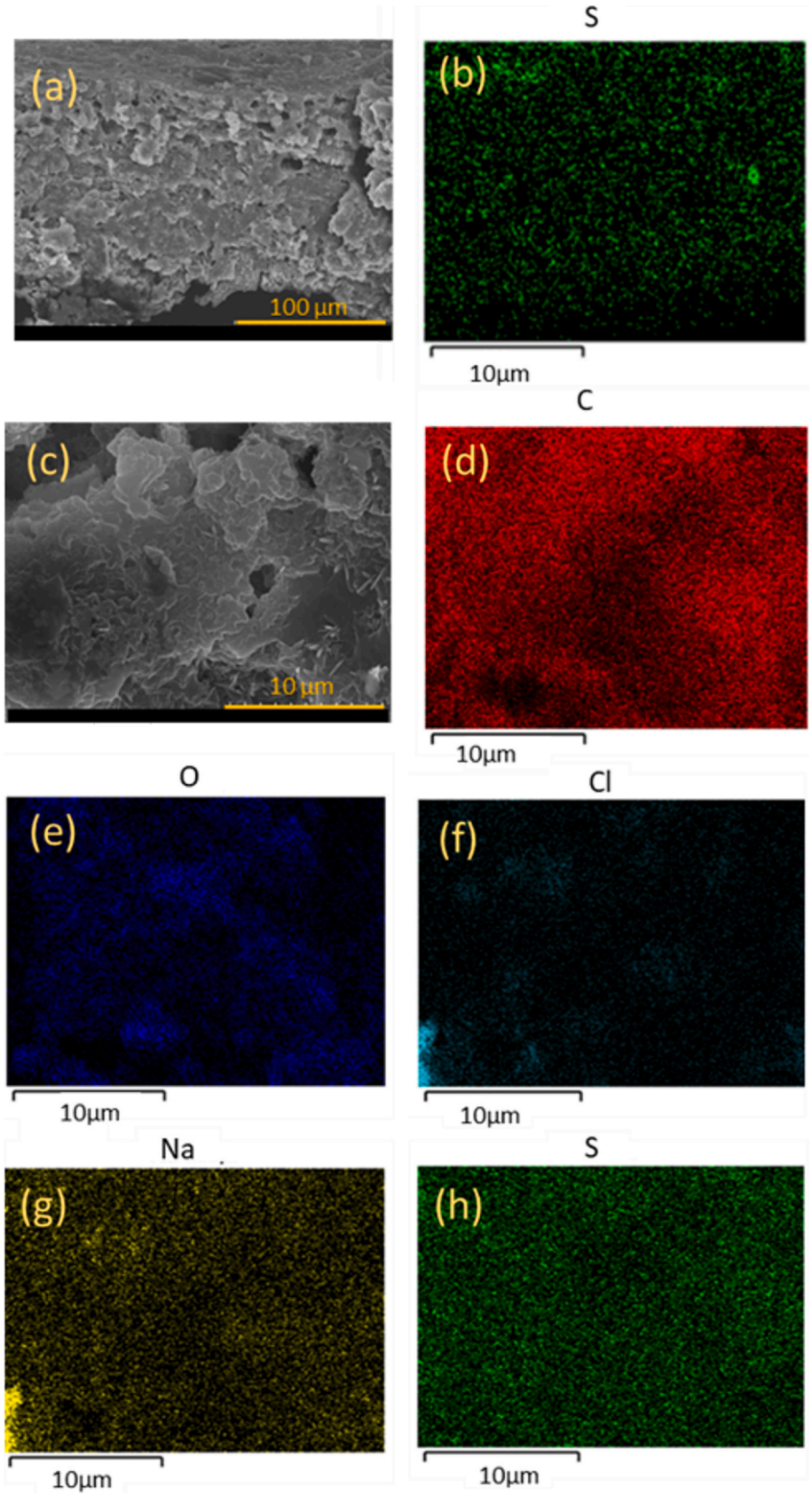

Fig. 7. SEM-EDS images of the STPE10 membrane (a) cross-section and (b) sulfur mapping, and of the STPE14 membrane (c) surface image and (d) carbon, (e) oxygen, (f) chlorine, (g) sodium and (h) sulfur mapping.

process. Further, the evaporation of the sulfonating medium initiates inter- and intramolecular crosslinking reactions within TPE and can lead to the formation of entangled sulfonate chains [46]. These unintentionally introduced sulfone cross-bridges decreases the effective degree of sulfonation by eliminating free sulfonic acid groups that promote cation exchange and increases the cross-linking density in a network that is already highly cross-linked (TPE polymer). This further inhibits the extra incorporation of the sulphonic acid groups into the polymer [45,47]. Therefore, till 14 h of sulfonation, there is a decrease in resistance as more cation exchange groups (sulfonic acid groups) are incorporated into the polymer backbone, but after 14 h, the resistance starts to increase due to crosslinking of those cation exchange groups and their conversion into sulfone cross-bridges.

3.2.6. *Assessment of chemical elements distribution by SEM-EDS*

Assessment of sulfur distribution in the membranes (equilibrated in 0.1 M NaCl) was done by elemental mapping. Fig. 7a and b show SEM-EDS images of the STPE10 membrane cross-section. The images confirm that sulfur has penetrated the membrane and that the membrane modification was uniform. Additionally, the surface SEM-EDS images of the STPE14 membrane also confirm an evenly distribution of sulfur throughout the surface of the membrane. The elemental mapping of the STPE14 membrane (Fig. 7c-h) also provides an interesting insight into the presence of sodium and chloride. Sodium and sulfur are present in almost equal quantities (1.94 and 1.79 atomic per cent) at the membrane surface, while the chlorine amount is just 0.55 atomic per cent, thus less than one-third of the quantity of sodium, which can be explained by Donnan exclusion of co-ions by the membrane. This data highlights that in the STPE14 membrane, sulfur is present in a sulfonic acid form, hence it could interact sodium to form $RSO_3^-Na^+$ ion-pair.

3.3. *Profiled membranes*

One of 3D printing's advantages is the possibility of manufacturing objects with complex designs. Thus, state-of-the-art chevron-profiled membranes and stripe-profiled membranes (Fig. 8) were manufactured to verify whether the proposed method allows for preparing such profiled cation-exchange membranes. Based on the optimisation done for flat membranes, the sulfonation time was 14 h.

Profiled membranes exhibited very similar mechanical properties to those of flat membranes, with an elongation percentage in the range of 106–307 % and yield points of 2.08 MPa and 1.53 MPa (with an error value of ± 50 Pa) for chevron and stripe profiled membranes, respectively. The results indicate the highly elastic nature of the profiled membranes. The chevron-profiled membrane shows an electrical resistance of 10.9 ± 2 Ωcm^2 and a permselectivity of 80.2 ± 4 %. The stripe-profiled membrane has an electrical resistance of 12.2 ± 2 Ωcm^2 and a permselectivity of 84.0 ± 4 %. These results demonstrate the effectiveness of the FDM 3D printing technique for fabricating profiled membranes, which can be functionalised into cation-exchange membranes. Furthermore, since FDM 3D printing does not require solvents and most reagents are consumed during sulfonation (Section 6 in the Supporting Information), the environmental factor (E-factor) is notably low (1.5) compared to traditional manufacturing methods, where it can reach up to 2000. Thus, the method developed and presented here offers a much greener and sustainable alternative for manufacturing cation-exchange membranes for electrochemical applications.

4. Conclusions

The fused deposition modelling (FDM) 3D printing method, followed by sulfonation of the obtained thermoplastic polymer elastomer (TPE) membranes (made of a combination of a polyolefin and styrene-ethylene-butylene), allowed for fabrication of flat, chevron- and stripe-profiled cation-exchange membranes, addressing the environmental drawbacks of conventional membrane manufacturing, particularly the generation of wastewater contaminated with toxic solvents. The 3D-printed membranes demonstrated electrochemical properties similar to those of commercial CEMs used in an increasing number of sustainable electromembrane processes. Sulfonation time had to be optimised

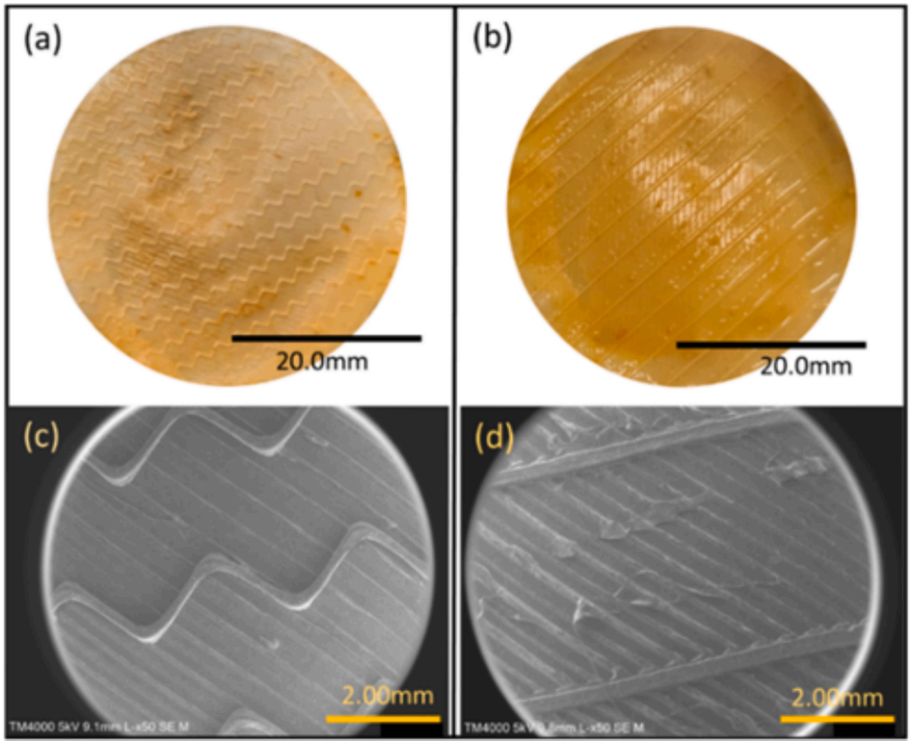

Fig. 8. Photos of (a) chevron and (b) stripe profiled cation exchange membranes (14 h sulfonation) and respective SEM images of their small section focused on (c) chevron and (d) stripe profile.

(herein, it was 14 h) to find a compromise between a high degree of sulfonation and over-sulfonation that leads to sulfone cross-bridging, which restricts cations' conductivity. Finally, the FDM 3D printing method is solvent-free, labour and time-effective, and it allows for mould-free preparation of profiled membranes with complex geometries. This formulation opens up opportunities for an easier and greener use of profiled membranes in various electromembrane processes, leading to intensified mass transfer and reduced energy consumption.

Declaration of competing interest

The authors declare that they have no known competing financial interests or personal relationships that could have appeared to influence the work reported in this paper.

Acknowledgements

This work was funded by the European Union through the project EXBRINER—HORIZON-MSCA-DN-2021, under the Marie Sklodowska-Curie grant agreement No 101072449 DOI 10.3030/101072449. This work was also financed by national funds from FCT - Fundação para a Ciência e a Tecnologia, I.P., under the scope of the project UID/50006/2023 of the Associate Laboratory for Green Chemistry - LAQV REQUIMTE. The authors would also like to acknowledge Dr H.M. Saif (NOVA FCT, Portugal) for constructing the cells used to measure membranes' permselectivity and electrical resistance and Prof. Vitor Alves (ISA, Portugal) for providing support to analyse the mechanical properties of the membranes.

Appendix A. Supplementary data

Supplementary data to this article can be found online at https://doi.org/10.1016/j.seppur.2025.134567.

Data availability

Data will be made available on request.

References

[1] D. Panarello, A. Gatto, Decarbonising Europe – EU citizens' perception of renewable energy transition amidst the European Green Deal, Energy Policy 172 (2023) 113272, https://doi.org/10.1016/j.enpol.2022.113272.
[2] S. Al-Amshawee, M.Y.B.M. Yunus, A.A.M. Azoddein, D.G. Hassell, I.H. Dakhil, H. A. Hasan, Electrodialysis desalination for water and wastewater: a review, Chem. Eng. J. 380 (2020) 122231, https://doi.org/10.1016/j.cej.2019.122231.
[3] G. Hopsort, Q. Cacciuttolo, D. Pasquier, Electrodialysis as a key operating unit in chemical processes: from lab to pilot scale of latest breakthroughs, Chem. Eng. J. 494 (2024) 153111, https://doi.org/10.1016/j.cej.2024.153111.
[4] S. Pawlowski, R.M. Huertas, C.F. Galinha, J.G. Crespo, S. Velizarov, On operation of reverse electrodialysis (RED) and membrane capacitive deionisation (MCDI) with natural saline streams: a critical review, Desalination 476 (2020) 114183, https://doi.org/10.1016/j.desal.2019.114183.
[5] Q. Xiao, J. Ma, L. Xu, K. Zuo, H. Guo, C.Y. Tang, Membrane capacitive deionization (MCDI) for selective ion separation and recovery: Fundamentals, challenges, and opportunities, J. Memb. Sci. 699 (2024) 122650, https://doi.org/10.1016/j.memsci.2024.122650.
[6] H.M. Saif, J.G. Crespo, S. Pawlowski, Lithium recovery from brines by lithium membrane flow capacitive deionization (Li-MFCDI) – a proof of concept, J. Membr. Sci. Lett. 3 (2023) 100059, https://doi.org/10.1016/j.memlet.2023.100059.
[7] H.M. Saif, T.H. Gebregeorgis, J.G. Crespo, S. Pawlowski, The influence of flow electrode channel design on flow capacitive deionization performance: Experimental and CFD modelling insights, Desalination 578 (2024) 117452, https://doi.org/10.1016/j.desal.2024.117452.
[8] H.M. Saif, J.G. Crespo, S. Pawlowski, Can 3D-printed flow electrode gaskets replace CNC-milled graphite current collectors in flow capacitive deionization? Desalination 597 (2025) 118362 https://doi.org/10.1016/j.desal.2024.118362.
[9] H.M. Saif, J.G. Crespo, S. Pawlowski, How should flow electrode capacitive deionization (FCDI) be operated to achieve efficient desalination and scalability? Desalination 606 (2025) 118769 https://doi.org/10.1016/j.desal.2025.118769.
[10] K. Ayers, The potential of proton exchange membrane–based electrolysis technology, Curr. Opin. Electrochem. 18 (2019) 9–15, https://doi.org/10.1016/j.coelec.2019.08.008.
[11] R.A. Tufa, S. Pawlowski, J. Veerman, K. Bouzek, E. Fontananova, G. di Profio, S. Velizarov, J. Goulão Crespo, K. Nijmeijer, E. Curcio, Progress and prospects in reverse electrodialysis for salinity gradient energy conversion and storage, Appl. Energy 225 (2018) 290–331, https://doi.org/10.1016/j.apenergy.2018.04.111.
[12] S. Pawlowski, J. Crespo, S. Velizarov, Sustainable Power Generation from Salinity Gradient Energy by Reverse Electrodialysis, in: A.B. Ribeiro, E.P. Mateus, N. Couto (Eds.), Electrokinet. Across Discip. Cont., Springer International Publishing, Cham, 2016: pp. 57–80. doi:10.1007/978-3-319-20179-5_4.
[13] S. Pawlowski, C.F. Galinha, J.G. Crespo, S. Velizarov, Prediction of reverse electrodialysis performance by inclusion of 2D fluorescence spectroscopy data into multivariate statistical models, Sep. Purif. Technol. 150 (2015) 159–169, https://doi.org/10.1016/j.seppur.2015.06.032.
[14] M. Razali, J.F. Kim, M. Attfield, P.M. Budd, E. Drioli, Y.M. Lee, G. Szekely, Sustainable wastewater treatment and recycling in membrane manufacturing, Green Chem. 17 (2015) 5196–5205, https://doi.org/10.1039/C5GC01937K.
[15] S. Depuydt, B. Van der Bruggen, Green Synthesis of Cation Exchange Membranes: a Review, Membranes 14 (2024) 23, https://doi.org/10.3390/membranes14010023.
[16] S. Pawlowski, J.G. Crespo, S. Velizarov, Profiled Ion Exchange Membranes: a Comprehensible Review, Int. J. Mol. Sci. 20 (2019) 165, https://doi.org/10.3390/ijms20010165.
[17] V. Vasil'eva, E. Goleva, N. Pismenskaya, A. Kozmai, V. Nikonenko, Effect of surface profiling of a cation-exchange membrane on the phenylalanine and NaCl separation performances in diffusion dialysis, Sep. Purif. Technol. 210 (2019) 48–59. doi:10.1016/j.seppur.2018.07.065.
[18] S. Pawlowski, V. Geraldes, J.G. Crespo, S. Velizarov, Computational fluid dynamics (CFD) assisted analysis of profiled membranes performance in reverse electrodialysis, J. Memb. Sci. 502 (2016) 179–190, https://doi.org/10.1016/j.memsci.2015.11.031.
[19] S. Pawlowski, T. Rijnaarts, M. Saakes, K. Nijmeijer, J.G. Crespo, S. Velizarov, Improved fluid mixing and power density in reverse electrodialysis stacks with chevron-profiled membranes, J. Memb. Sci. 531 (2017) 111–121, https://doi.org/10.1016/j.memsci.2017.03.003.
[20] D.A. Vermaas, M. Saakes, K. Nijmeijer, Power generation using profiled membranes in reverse electrodialysis, J. Memb. Sci. 385–386 (2011) 234–242, https://doi.org/10.1016/j.memsci.2011.09.043.
[21] Z.X. Liang, T.S. Zhao, C. Xu, J.B. Xu, Microscopic characterizations of membrane electrode assemblies prepared under different hot-pressing conditions, Electrochim. Acta 53 (2007) 894–902, https://doi.org/10.1016/j.electacta.2007.07.071.
[22] M. Yao, Y.C. Woo, L.D. Tijing, W.-G. Shim, J.-S. Choi, S.-H. Kim, H.K. Shon, Effect of heat-press conditions on electrospun membranes for desalination by direct contact membrane distillation, Desalination 378 (2016) 80–91, https://doi.org/10.1016/j.desal.2015.09.025.
[23] M.J. Nategh, B. Jafari, Experiments with a Low-cost Hot Isothermal Pressing Machine developed for Superplastic Forming, J. Mater. Eng. Perform. 17 (2008) 682–687, https://doi.org/10.1007/s11665-008-9213-9.
[24] N. Yanar, P. Kallem, M. Son, H. Park, S. Kang, H. Choi, A New era of water treatment technologies: 3D printing for membranes, J. Ind. Eng. Chem. 91 (2020) 1–14, https://doi.org/10.1016/j.jiec.2020.07.043.
[25] L.D. Tijing, J.R.C. Dizon, I. Ibrahim, A.R.N. Nisay, H.K. Shon, R.C. Advincula, 3D printing for membrane separation, desalination and water treatment, Appl. Mater. Today 18 (2020) 100486, https://doi.org/10.1016/j.apmt.2019.100486.
[26] X. Yu, H. Yang, X. Lv, X. Zhang, V. Jegatheesan, X. Zhou, Y. Zhang, Characterization and Performance Evaluation of Digital Light Processing 3D Printed Functional Anion Exchange Membranes in Electrodialysis, Processes 12 (2024) 1043, https://doi.org/10.3390/pr12061043.
[27] L. Zárybnická, Z. Meloun, J. Šafka, V. Truxová, K. Dvořák, J. Machotová, 3D printed heterogeneous cation exchange membrane processed using stereolithography, J. Appl. Polym. Sci. 140 (2023) 1–9, https://doi.org/10.1002/app.54341.
[28] J. Seo, D.I. Kushner, M.A. Hickner, 3D Printing of Micropatterned Anion Exchange Membranes, ACS Appl. Mater. Interfaces 8 (2016) 16656–16663, https://doi.org/10.1021/acsami.6b03455.
[29] C. Capparelli, C.R. Fernandez Pulido, R.A. Wiencek, M.A. Hickner, Resistance and Permselectivity of 3D-printed Micropatterned Anion-Exchange Membranes, ACS Appl. Mater. Interfaces 11 (2019) 26298–26306, https://doi.org/10.1021/acsami.8b04177.
[30] N. Yu, J. Dong, H. Li, T. Wang, J. Yang, Improving the performance of quaternized SEBS based anion exchange membranes by adjusting the functional group and side chain structure, Eur. Polym. J. 154 (2021) 110528, https://doi.org/10.1016/j.eurpolymj.2021.110528.
[31] J.-E. Yang, J.-S. Lee, Selective modification of block copolymers as proton exchange membranes, Electrochim. Acta 50 (2004) 617–620, https://doi.org/10.1016/j.electacta.2004.03.064.
[32] H.-S. Park, C.-K. Hong, Anion Exchange Membrane based on Sulfonated Poly (Styrene-Ethylene-Butylene-Styrene) Copolymers, Polymers 13 (2021) 1669, https://doi.org/10.3390/polym13101669.
[33] R. Rickert, R. Klein, F. Schönberger, Form-Stable phase Change Materials based on SEBS and Paraffin: Influence of Molecular Parameters of Styrene-b-(Ethylene-co-Butylene)-b-Styrene on Shape Stability and Retention Behavior, Materials 13 (2020) 3285, https://doi.org/10.3390/ma13153285.
[34] P. Dlugolecki, K. Nymeijer, S. Metz, M. Wessling, Current status of ion exchange membranes for power generation from salinity gradients, J. Memb. Sci. 319 (2008) 214–222, https://doi.org/10.1016/j.memsci.2008.03.037.

[35] H.Y. Hwang, H.C. Koh, J.W. Rhim, S.Y. Nam, Preparation of sulfonated SEBS block copolymer membranes and their permeation properties, Desalination 233 (2008) 173–182, https://doi.org/10.1016/j.desal.2007.09.040.
[36] Q. Wang, Y. Lu, N. Li, Preparation, characterization and performance of sulfonated poly(styrene-ethylene/butylene-styrene) block copolymer membranes for water desalination by pervaporation, Desalination 390 (2016) 33–46, https://doi.org/10.1016/j.desal.2016.04.005.
[37] M. Yan, Y. Lu, N. Li, F. Zeng, Q. Wang, H. Bai, Z. Xie, Hyperbranch-Crosslinked S-SEBS Block Copolymer Membranes for Desalination by Pervaporation, Membranes 10 (2020) 277, https://doi.org/10.3390/membranes10100277.
[38] C. del Río, O. García, E. Morales, P.G. Escribano, Single cell performance and electrochemical characterization of photocrosslinked and post-sulfonated SEBS-DVB membranes, Electrochim. Acta 176 (2015) 378–387, https://doi.org/10.1016/j.electacta.2015.07.009.
[39] J. Kerres, W. Cui, R. Disson, W. Neubrand, Development and characterization of crosslinked ionomer membranes based upon sulfinated and sulfonated PSU crosslinked PSU blend membranes by disproportionation of sulfinic acid groups, J. Memb. Sci. 139 (1998) 211–225, https://doi.org/10.1016/S0376-7388(97)00253-6.
[40] S.-Y. Jang, S.-H. Han, Characterization of sulfonated polystyrene-block-poly(ethyl-ran-propylene)-block-polystyrene copolymer for proton exchange membranes (PEMs), J. Memb. Sci. 444 (2013) 1–8, https://doi.org/10.1016/j.memsci.2013.04.055.
[41] J. Kim, B. Kim, B. Jung, Proton conductivities and methanol permeabilities of membranes made from partially sulfonated polystyrene-block-poly(ethylene-ran-butylene)-block-polystyrene copolymers, J. Memb. Sci. 207 (2002) 129–137, https://doi.org/10.1016/S0376-7388(02)00138-2.
[42] A. Lejarazu-Larrañaga, J.M. Ortiz, S. Molina, S. Pawlowski, C.F. Galinha, V. Otero, E. García-Calvo, S. Velizarov, J.G. Crespo, Nitrate Removal by Donnan Dialysis and Anion-Exchange Membrane Bioreactor using Upcycled End-of-Life reverse Osmosis Membranes, Membranes 12 (2022) 101, https://doi.org/10.3390/membranes12020101.
[43] M.G. Buonomenna, J. Bae, Block Copolymer-based Symmetric Membranes for Direct Methanol fuel Cells, Symmetry 16 (2024) 1079, https://doi.org/10.3390/sym16081079.
[44] Y. Hu, L. Yan, B. Yue, Chain-scission degradation mechanisms during sulfonation of aromatic polymers for PEMFC applications, Chem. Phys. 541 (2021) 111049, https://doi.org/10.1016/j.chemphys.2020.111049.
[45] C. Dalla Valle, M. Zecca, F. Rastrelli, C. Tubaro, P. Centomo, Effect of the Sulfonation on the Swollen State Morphology of Styrenic Cross-Linked Polymers, Polymers 12 (2020) 600, https://doi.org/10.3390/polym12030600.
[46] N.P. Valkanas, V.D. Vrekou, A.G. Theodoropoulos, G.N. Valkanas, I. C. Konstantakopoulos, Cross-linking regulators in one-step synthesis of macronet ion-exchangers, J. Mater. Sci. 31 (1996) 4831–4836, https://doi.org/10.1007/BF00355868.
[47] A.G. Theodoropoulos, V.T. Tsakalos, G.N. Valkanas, Sulfone-type crosslinks in sulfonation of macronet polystyrene backbone, Polymer (guildf). 34 (1993) 3905–3910, https://doi.org/10.1016/0032-3861(93)90518-F.